ACS Catalysis

Research Article

pubs.acs.org/acscatalysis

Small-Molecule Activation Driven by Confinement Effects

Julibeth M. Martinez de la Hoz and Perla B. Balbuena*

Department of Chemical Engineering and Department of Materials Science and Engineering Texas A&M University, College Station, Texas 77843, United States

Supporting Information

ABSTRACT: Electron-rich environments may arise from interactions between nanostructures at subnanometer separations and have been shown able to facilitate molecular dissociation of simple diatomic molecules. Electrons in these regions have energies close to the Fermi energy of the structures contributing to the electron-rich environment. These energies can be tuned to achieve specific interactions with the LUMO of molecules of interest. In this work, we focus on electron-rich regions generated between platinum nanoclusters and carbon nanotubes in the confined space defined by a nanopillared graphene (NPG) structure decorated with Pt_{22} nanoparticles. First, the reactivity of these regions is evaluated using density functional theory by comparing the bond strengths of O_2, CO, and N_2 adsorbed on Pt_{22} with that of the molecules adsorbed on similar surfaces in absence of surrounding electron-rich regions. Results show larger charge transfer to the adsorbed molecules in the presence of the electron-rich environments. These excesses of charge are located in molecular antibonding LUMO orbitals, thus weakening their molecular bonds and facilitating their dissociation. Second, the dissociation of O_2 and CH_4 molecules is investigated in the proposed Pt_{22}/NPG structure at different temperature and pressure conditions and compared with that taking place in a larger-pore-size Pt_{26}/graphite system using ab initio molecular dynamics simulations. The presence of the electron-rich regions may affect O_2 dissociation via two mechanisms: (a) generating wider spectra of charges available for transfer to adsorbed O_2 molecules which results in bond-length oscillations that facilitate molecular dissociation; (b) increasing the amount of charge transferred to adsorbed molecules, debilitating their molecular bond. On the other hand, when gas phase methane is exposed to electron-rich environments, it is found that the larger barrier between the Fermi energy of the system and the LUMO orbital of CH_4 impedes the interaction of the electron-rich regions with the molecular LUMO. However, enhanced reactivity driven by the confined nature of the electron-rich environment in Pt_{22}/NPG could also arise in this case as a result of a geometric effect, inducing an increased frequency of interaction between catalysts and molecules.

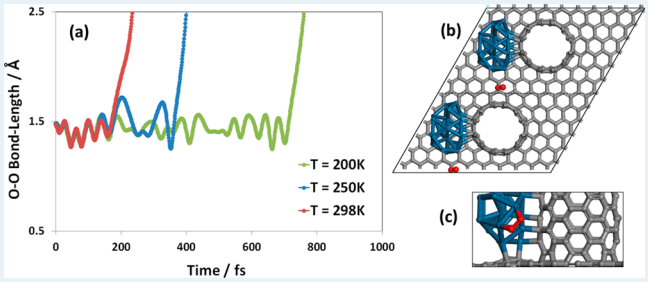

KEYWORDS: *density functional theory, confined geometries, nanomaterials, electron-rich environments, molecular dissociation, methane activation*

1. INTRODUCTION

Finite electronic densities have been found in the gap between metallic nanostructures separated by subnanometer distances due to migration of some of the conduction electrons into the interparticle region.[1−10] The effect of this electron-rich environment on the catalytic activity of transition metals has been investigated in previous works using density functional theory (DFT) and ab initio methods, modeling the system by two metallic thin films separated by distances between 4 and 7 Å.[1−3] Results showed that the dissociation of simple diatomic molecules is facilitated when taking place between the two metallic thin films, compared with those taking place on single surfaces. The main reason for this difference is the higher charge transferred to adsorbed molecules during their dissociation in the former case, which debilitates molecular bonds and facilitates bond-breaking processes. As a result, a direct relationship exists between the additional charge transferred to molecules and the decrease found in activation barriers for bond breaking.[2] In addition, the energies of the electrons present in the gap region were found to depend on the Fermi level (E_F) of the specific metal forming the pore, and they were shown to be within 5 eV of E_F.[3] Consequently, it was concluded that electronic coupling between electrons in the gap and the dissociating molecule may be controlled by tuning the nature and structure of materials from which electrons are migrating.

How can these new phenomena be found in practical catalytic structures? Given the catalytic enhancement promoted by electron-rich environments, it is of special interest to incorporate them as building blocks of suitable three-dimensional nanostructures. In this way, new catalytic materials with enhanced reactivity toward specific reactions can be obtained. The main requirements that a porous nanostructure can fulfill to be considered as a scaffold for the incorporation of these

Received: September 12, 2014
Revised: November 19, 2014
Published: November 25, 2014

regions are good stability, high surface area, and facile tailoring of pore sizes. One interesting three-dimensional material satisfying all of these conditions is nanopillared graphene (NPG), a novel nanostructure composed of parallel graphene layers connected by vertically aligned single-walled carbon nanotubes (SWCNTs).[11] In addition to graphene and SWCNTs having very similar crystal structures, SWCNTs are connected to the graphene layer through covalent bonds, providing NPG with the required stability.[12,13] In addition, experimental reports have measured high BET specific surface areas for these nanostructures (up to 2600 m^2/g),[12] comparable to the theoretical value for graphene and open-ended SWCNTs (2630 m^2/g).[14] Furthermore, the length of SWCNTs and the intertube distances can be easily tuned by changing variables during the synthesis process. For chemical vapor deposition-based synthesis, the precursor gas employed, deposition time, and catalyst nanoparticle diameter influence the growth rate and spacing of SWCNTs on the material.[13,15,16] NPG structures have been proposed mainly for applications related to hydrogen storage,[11] supercapacitors,[16,17] and nanoelectronics.[18] N-doped NPG has been assessed as an electrocatalyst for the oxygen reduction reaction in fuel cells,[19,20] and NPG structures decorated with metallic nanoparticles have been proposed for magnetic drug delivery applications[21] and as field emission devices.[22]

In this work, a Pt-decorated NPG structure exhibiting electron-rich regions is proposed as a nanostructured catalyst for the dissociation of molecules in gas phase. Electron-rich regions are present in confined spaces formed by two nanostructures interacting at separations between 4 and 7 Å.[1−10] Therefore, nanopores with sizes between 4 and 7 Å must be present in our proposed nanocatalyst. Other ordered carbon materials decorated with metallic nanoparticles have been suggested in the past as electrocatalysts in fuel cell reactions. For example, ordered mesoporous carbon decorated with Pt and Pt−Ru nanoparticles have been tested as electrocatalysts for methanol oxidation and have shown enhanced electrochemical performance in comparison with commercial catalysts;[23−25] however, the average pore sizes in those carbon-based catalysts are on the order of tens of nanometers. The novelty of our work is based on the incorporation of electron-rich regions in confined spaces defined by the metal/carbon nanostructure. It is expected that the existence of such regions leads to interactions between electrons and gas-phase adsorbates beyond those given by surface effects, resulting in the weakening of molecular bonds and an enhancement of the reactivity of the material.

In this work, first a suitable NPG structure decorated with Pt-nanoclusters and exhibiting electron-rich regions is proposed, and its catalytic activity is investigated using DFT by evaluating bond strengths of diatomic molecules. Second, the dissociation of oxygen and methane molecules on Pt-decorated NPG is evaluated using ab initio molecular dynamics (AIMD) simulations. In this way, enhancements on the reactivity given by the presence of electron-rich regions can be directly observed under various temperature/pressure conditions.

2. COMPUTATIONAL AND SYSTEM DETAILS

2.1. Metal-Decorated NPG Structure. The NPG structure was built following the procedure described by Dimitrakakis et al.[11] A 6 × 10 graphene sheet was optimized along with a (6, 6) SWCNT with DFT methods, resulting in the formation of covalent bonds between the graphene substrate and the SWCNT (Figure 1). To decorate the resulting NPG structure with Pt nanoparticles, two different

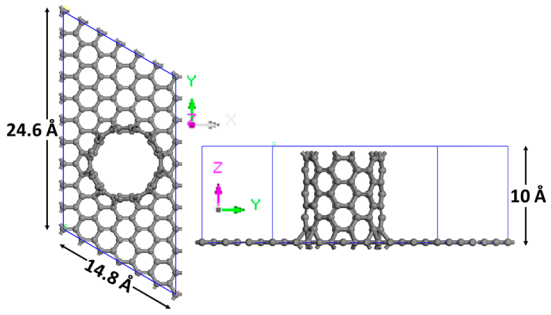

Figure 1. Unit cell of the NPG structure built following the procedure described by Dimitrakakis et al. Left: top view. Right: lateral view.

approaches were taken. In the first one, two Pt_{13} clusters were adsorbed onto the SWCNT, with an initial separation of 6.5 Å between their periodic images (Figure 2a). In this arrangement, the metallic clusters interacting with each other at distances between 4 and 7 Å resemble the interacting thin films studied earlier.[1−3] In the second approach, one Pt_{22} cluster was adsorbed onto the structure with an initial separation of 5.6 Å from the SWCNT periodic image (Figure 2b). In this case, the electron-rich environment is expected to be formed through the interaction between metallic clusters and SWCNTs at distances between 4 and 7 Å.

SWCNTs are formed by rolling up graphene layers to form a tubular structure. Carbon atoms in graphene interact with each other through strong σ-bonds, to which each atom contributes three electrons. The fourth electron is in the p_z orbital, which extends vertically above and below the plane, forming the π bonding and the π^* antibonding states. Electrons in these unbound states may be susceptible to migration to a gap formed by a metallic surface interacting with graphene at very short distances (4−7 Å). In addition, the SWCNT's curvature generates a shifting of electrons from the π orbital to the convex outer surface of the tube, which can further facilitate the formation of an electron-rich region between a metallic cluster and the SWCNT.[26] The electronic density in this region is quantified by calculating the number of electrons in the systems shown in Figure 3.

2.2. Adsorption of Diatomic Molecules in Electron-Rich Regions of Metal-Decorated NPG. To evaluate the effect that electron-rich regions may have on the reactivity of Pt-decorated NPG, the diatomic molecules O_2, N_2, and CO were adsorbed onto a Pt_{26} cluster, and their bond lengths and charges were evaluated for cases with and without the presence of electron-rich environments. These regions are formed by the interaction between Pt_{26} and graphene at H = 4.9 Å and H = 15 Å, respectively (Figure 3a). The O_2 molecule was adsorbed horizontally on a bridge configuration, similar to the $t-b-t$ stable configuration found for the molecule adsorbed on Pt(111).[27] A similar configuration was adopted in the case of N_2. In the case of CO, the molecule was adsorbed vertically through the C atom on a bridge site of the nanocluster. This configuration was theoretically found as one of the most stables for CO adsorption on Pt(111).[28] The adsorption configuration for each molecule was exactly the same for both separations (H = 4.9 and 15 Å). Thus, differences in their bond strength reflect exclusively the effect of the electron-rich environment (present for H = 4.9 Å).

dx.doi.org/10.1021/cs5013798 | ACS Catal. 2015, 5, 215−224

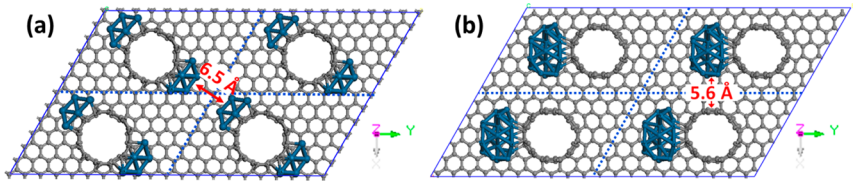

Figure 2. (a) Top view of four unit cells of a proposed NPG structure decorated using two Pt_{13} clusters. (b) Top view of four unit cells of a proposed decorated NPG structure using one Pt_{22} cluster. Carbon atoms are gray and platinum atoms are blue.

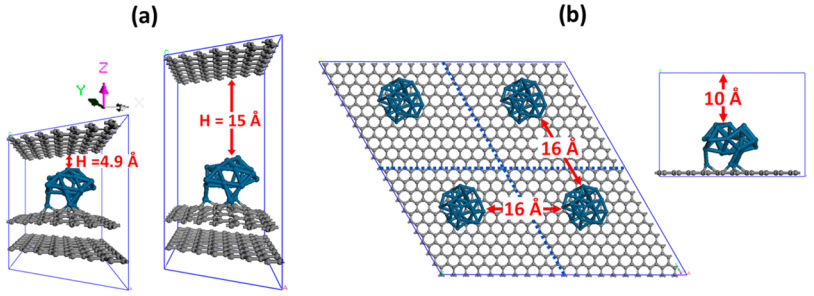

Figure 3. (a) Unit cell of a Pt_{26} cluster interacting with graphene at H = 4.9 Å (left) and H = 15 Å (right). (b) Pt_{26} cluster over a graphene sheet. Left: top view of four unit cells. Right: lateral view of the unit cell. Carbon atoms are gray and platinum atoms are blue.

2.3. Stability of Adsorbed O_2 on Pt_{22}/NPG. To evaluate the influence of electron-rich regions on the dissociation of O_2 on Pt_{22}/NPG at different (T, P) conditions, simulations were performed at three state points: (200 K, 10 atm), (250 K, 13 atm), and (298 K, 15 atm). In all cases, the density (ρ) of O_2 in the systems was held constant at 19.5 kg/m^3, and the resulting pressure was calculated using tables of thermodynamic properties of O_2 at the given (T, ρ) conditions.[29] One oxygen molecule was needed to reproduce this density on the Pt_{22}/NPG system shown in Figure 2b. Simulations carried out on this system were then compared to those of three oxygen molecules (ρ = 19.5 kg/m^3) interacting with the Pt_{26}/graphite system shown in Figure 3b at the same (T, P) conditions.

The system in Figure 3b represents an ordered carbon-based material with larger pore sizes than those in NPG (~1 nm vs ~0.56 nm in NPG), and consequently, electron-rich regions are not present. Experimentally, ordered mesoporous carbon materials decorated with platinum nanoparticles (pore sizes between 2 and 50 nm) may be synthesized by using mesoporous silicates such as SBA-15.[23−25] Results obtained in this section will enable elucidating the effect of electron-rich regions on the reactivity of platinum-decorated microporous carbon materials.

2.4. Adsorption and Stability of Adsorbed CH_4 on Pt_{22}/NPG. Methane is the main component of natural gas, and it is widely used in industry for obtaining hydrogen, higher hydrocarbons, and oxygenates such as alcohols and formaldehydes; however, methane is a highly stable molecule, requiring high energies to activate its C−H bond (104 kcal/mol).[30] Steam reforming is one of the most commonly used processes in industry to activate it to obtain syngas, but this process has to be performed at high temperatures (>1000 K) and medium pressures (~30 atm), which makes it significantly expensive;[31] hence, it is very important to propose effective strategies to activate methane at milder conditions. Results in this section will help elucidate if methane dehydrogenation on Pt/NPG structures is facilitated, thus reducing (T, P) conditions at which the reaction takes place.

To evaluate how electron-rich regions influence the dissociation of CH_4 on Pt_{22}/NPG at different (T, P) conditions, simulations were performed at four state points: (1000 K, 300 atm), (1100 K, 329 atm), (1200 K, 359 atm), and (1500 K, 449 atm). In all cases, the density (ρ) of CH_4 in the systems was held constant at 58.6 kg/m^3, and the resulting pressure was calculated using the ideal gas equation for the given (T, ρ) conditions. Six methane molecules were needed to reproduce this density on the Pt_{22}/NPG system shown in Figure 2b, and 19 molecules reproduce this density on the Pt_{26}/graphite system shown in Figure 3b.

Dehydrogenation of molecules such as methyl cyclohexane has been carried out successfully using Pt nanoparticles confined on the pores on ordered SBA-15 templates, and higher catalytic activities were reported for this system compared with those of conventional Pt/SiO_2.[32] The reasons for this are mainly attributed to the more homogeneous dispersion of Pt nanoparticles on the ordered SBA-15 substrate and the restriction in the growth of Pt nanoparticles inside the pore of SBA-15 (methyl cyclohexane dehydrogenation is particle-size-dependent). Consequently, ordered Pt/NPG catalysts may be good candidates for the dehydrogenation of methane at milder (T, P) conditions.

2.5. General Computational Details. Calculations were performed using the Vienna ab initio simulation package VASP,[33−37] with the revised Perdew−Burke−Ernzerhof functional (GGA-rPBE)[38] and the projector augmented wave (PAW) pseudopotentials provided in the VASP databases describing electron−ion interactions.[39,40] The plane wave was expanded up to a cutoff energy of 400 eV. The convergence criteria for ionic relaxation loop and for electronic self-consistent iteration were set to 10^{-3} and 10^{-4} eV, respectively. A Gaussian smearing with a width of 0.2 eV was employed, and a 4 × 4 × 1 k-points Monkhorst−Pack[41] mesh sampling was used in the surface Brillouin zone. AIMD simulations were carried out using the NVT ensemble with a time step of 1 fs. The Nose thermostat was used to control the temperature oscillations during the simulation with a Nose mass parameter of 0.5, which gives a frequency of oscillation corresponding to 176 time steps. A Γ-point Brillouin zone sampling with a plane wave energy cutoff of 400 eV was applied in this case. All of the systems were allowed to run at least 8 ps. Bader charge analyses

dx.doi.org/10.1021/cs5013798 | ACS Catal. 2015, 5, 215−224

were used to perform charge calculations.[42,43] Within this method, the total electronic charge of an atom is approximated by the charge enclosed within the Bader volume defined by zero flux surfaces.

3. RESULTS

3.1. Characterization of Electron-Rich Regions in Metal-Decorated NPG Structure. The Pt-decorated NPG structure proposed in Figure 2a is shown in Figure S-1 (Supporting Information) after DFT optimization. The two Pt_{13} clusters separated by very short distances (<7 Å) interact strongly and end up merging during the geometry optimization. In contrast, the structure of the Pt-decorated NPG proposed in Figure 2b is well maintained, and the final separation between the Pt_{22} cluster and the SWCNT slightly changes from 5.6 to 5.5 Å. Because the structure of the Pt-decorated NPG in Figure 2b is stable and small pores are formed between Pt and SWCNTs (pore size: 5.5 Å), this nanostructure is chosen as the model catalyst to be used in our reactivity studies.

To quantify the number of electrons in electron-rich regions formed by a Pt cluster and a graphene sheet, DFT calculations were performed to calculate the number of electrons in a gap formed by a Pt_6 cluster and a graphene layer 5 Å apart (Figure 4, left). In addition, this number was compared with that

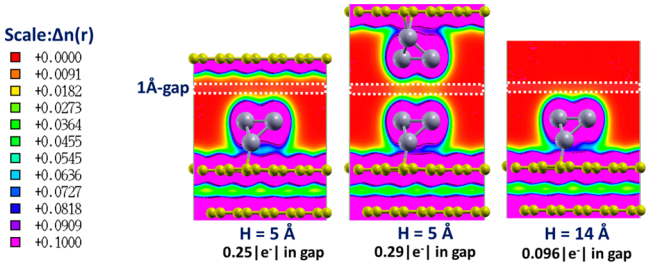

Figure 4. Electronic density in a gap formed by a Pt_6 cluster and a graphene layer 5 Å apart (left), two Pt_6 clusters 5 Å apart (center), and one Pt_6 cluster over a graphene sheet (right). Carbon atoms are yellow and platinum atoms are gray. Color code for the electronic density is shown in the table.

calculated using two Pt_6 clusters separated by 5 Å (Figure 4, center) and to the one calculated using only one Pt_6 cluster over a graphene sheet (Figure 4, right). The number of electrons was calculated in a 1 Å subgap region (as shown in Figure 4) defined in the gap between the nanostructures. Figure 4 also depicts the electronic density in each system after the DFT optimization. The calculated number of electrons in the gap formed by platinum and graphene is just 14% smaller than that in the gap formed by platinum clusters (0.25 vs 0.29 electrons). It is also interesting to note that the number of electrons in the same gap region for a platinum cluster over graphene (Figure 4, right) is very close to zero, confirming that the calculated number of electrons in the gap for the other two systems is a result of tunneling of electrons as a result of close interaction between the nanostructures at small separations.

Calculations in this section demonstrate that Pt-decorated NPG structures (Figure 2b) possess electron-rich regions in the small gaps formed by metal clusters interacting with carbon nanotubes. The effect of electron-rich regions on the reactivity of Pt-decorated NPG structures is discussed in the next section.

3.2. Adsorption of Diatomic Molecules in Electron-Rich Regions of Metal-Decorated NPG. The final configurations of O_2, N_2, and CO molecules adsorbed onto the Pt_{26}/graphite systems in Figure 3a are shown in Figure 5,

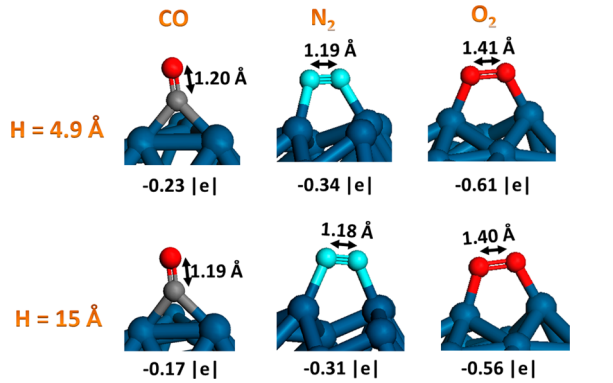

Figure 5. Final configurations of O_2, N_2, and CO molecules adsorbed onto the Pt_{26}/graphite systems in Figure 3a. Bond lengths and charges in each case are also shown. Platinum atoms are blue, carbon atoms are gray, nitrogen atoms are light blue, and oxygen atoms are red.

along with their bond lengths and charges of adsorbed molecules in each system. Charges transferred to molecules in electron-rich regions (H = 4.9 Å) during adsorption are up to 35% larger compared with those of molecules adsorbed on the cluster with no electron-rich regions (H = 15 Å). In addition, bond lengths of adsorbed molecules are up to 0.84% longer in electron-rich regions. This reflects weaker molecular bonds resulting from the larger number of charge transferred to molecules and possibly smaller barriers for their dissociation in electron-rich regions. The lowest unoccupied molecular orbital (LUMO) of O_2, N_2, and CO is an antibonding orbital, and its additional filling weakens the molecular bond.[44,45] In fact, previous calculations on Pt(111) surfaces showed that O_2 molecules receiving 0.11 more electrons during their adsorption in electron-rich environments required 39% less energy to be dissociated than those adsorbed without the presence of electron-rich regions (activation barrier 0.25 eV smaller). Analogously, CO molecules receiving 0.14 more electrons required 6.4% less energy to be dissociated (activation barrier 0.27 eV smaller).[2]

In the cases studied in this work, O_2 and CO molecules adsorbed on Pt_{26} clusters in the presence of electron-rich environments received 0.06 and 0.05 more electrons that their counterparts adsorbed on the cluster with no electron-rich environments. These increases in charge correspond to 54 and 36% of those calculated for O_2 and CO on electron-rich Pt(111). Therefore, noticeable reductions in activation barriers are also expected when such molecules are adsorbed on Pt-NPG in the presence of electron-rich regions compared with barriers on Pt-NPG structures with no electron-rich regions present.

It is interesting to note a variation in the magnitude of the charges shown in Figure 5 for each molecule. Given the importance of the charge transferred to the molecule during its adsorption on the weakening of its molecular bond and the facilitation of its dissociation, it is vital to understand the origin of such differences. To accomplish this, the Fermi level of the Pt_{26}/graphite system in Figure 3a was calculated and compared with the LUMO of the three different molecules studied: O_2, N_2, and CO. Figure 6 (left) shows the calculated values, relative to the energy levels of vacuum. An effective coupling between

dx.doi.org/10.1021/cs5013798 | ACS Catal. 2015, 5, 215−224

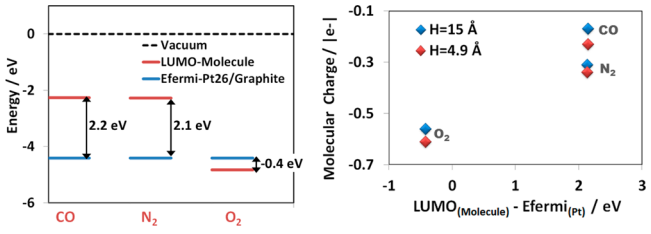

Figure 6. Left: Fermi level of the Pt_{26}/graphite system in Figure 3a (blue line) compared with the LUMOs of O_2, N_2, and CO (red line). Right: charges of O_2, N_2, and CO molecules adsorbed on Pt_{26}/graphite as a function of the barrier (LUMO molecule − $E_{Fermi\text{-}Pt_{26}}$).

Fermi energy and LUMO is expected to result in better electron transfer. Specifically, the difference (energy of $LUMO_{molecule} - E_{Fermi\text{-}Pt_{26}}$) provides the barrier required for charge transfer to the molecule.

In the case of the O_2 molecule, the LUMO lies below the Fermi energy of Pt_{26}/graphite, which allows for a spontaneous transference of charge from the cluster. In contrast, the LUMO energies of N_2 and CO are above the Fermi level of Pt_{26}/graphite, which gives rise to barriers in charge transfer corresponding to 2.1 and 2.2 eV, respectively. These results are consistent with the charges calculated for the different molecules adsorbed on Pt_{26}/graphite at both separations, H = 4.9 and H = 15 Å (Figure 5). The largest charge transfer is found for O_2, which has no barrier for the transference of electrons to its LUMO, followed by N_2 (barrier: 2.1 eV) and CO (barrier: 2.2 eV). As mentioned above, the LUMO of these molecules corresponds to an antibonding orbital, and filling such orbital facilitates their dissociation. Figure 6 (right) shows the charges of O_2, N_2, and CO adsorbed on Pt_{26}/graphite as a function of the energy barrier ($LUMO_{molecule} - E_{Fermi\text{-}Pt_{26}}$). It is clear from the graph that smaller ($LUMO_{molecule} - E_{Fermi\text{-}Pt_{26}}$) energy differences result in a larger amount of (negative) charges transferred to adsorbed molecules. The same trend is observed in systems with and without the presence of electron-rich regions (H = 4.9 and H = 15 Å, respectively). However, the effect of the electron-rich region is reflected in an increased number of electrons being transferred to the molecule.

These results are important for the design of metal-decorated NPG catalysts with enhanced reactivity toward specific reactions. NPG systems can be decorated with metal clusters whose Fermi energy effectively couples with the LUMO of molecules of interest (small or negative $LUMO_{molecule} - E_{Fermi\text{-}Pt_{26}}$ differences). In that way, a larger amount of charge can be transferred to the molecular LUMO orbitals, facilitating their dissociation. If electron-rich regions are present, this study shows that the amount of charge being transferred to the molecule of interest is further increased, enhancing the reactivity of the nanostructured material.

3.3. Effect of Pore Size on O_2 Reactivity over Pt-Decorated Microporous Carbon Structures. Figure 7a shows the O−O bond length as a function of time for the O_2 molecule interacting with the smallest-pore microporous Pt_{22}/NPG system at (200 K, 10 atm), (250 K, 13 atm), and (298 K, 15 atm). Time zero represents the time at which the molecule is first adsorbed onto the Pt_{22} nanoparticle. In all cases, the initial configuration corresponded to the O_2 molecule in the gap between the Pt_{22} cluster and the SWCNT, at ∼3 Å of the Pt nanoparticle (Figure 7b). After adsorption, the O_2 molecule is on a bridge site interacting with two platinum atoms, as shown in Figure 7c. As expected, increasing the temperature decreases the time required to observe dissociation of the adsorbed O_2 molecule. This time corresponds to 710, 370, and 170 fs at 200, 250, and 298 K, respectively (Figure 7a).

Adsorption of O_2 molecules at the same (T, P) conditions was also studied on the larger-pore Pt_{26}/graphite system in Figure 3b. After 8 ps of AIMD simulations all of the oxygen molecules get adsorbed onto the Pt_{26} cluster. However, none of the molecules dissociated at any of the conditions studied. Figure 8 shows the final configuration of the systems at (200 K, 10 atm), (250 K, 13 atm), and (298 K, 15 atm).

To understand the observed differences in reactivity between Pt_{22}/NPG (small pore size) and Pt_{26}/graphite (larger pore size), the O−O bond lengths of the molecule adsorbed on Pt_{22}/NPG are compared at each (T, P) condition with those of the O_2 molecule adsorbed on the bridge configuration on Pt_{26}/graphite as a function of time (Figure 9). Again, time zero represents the time at which the molecule is first adsorbed onto the Pt nanoparticle (Pt_{22} or Pt_{26}). It is evident that for T = 200

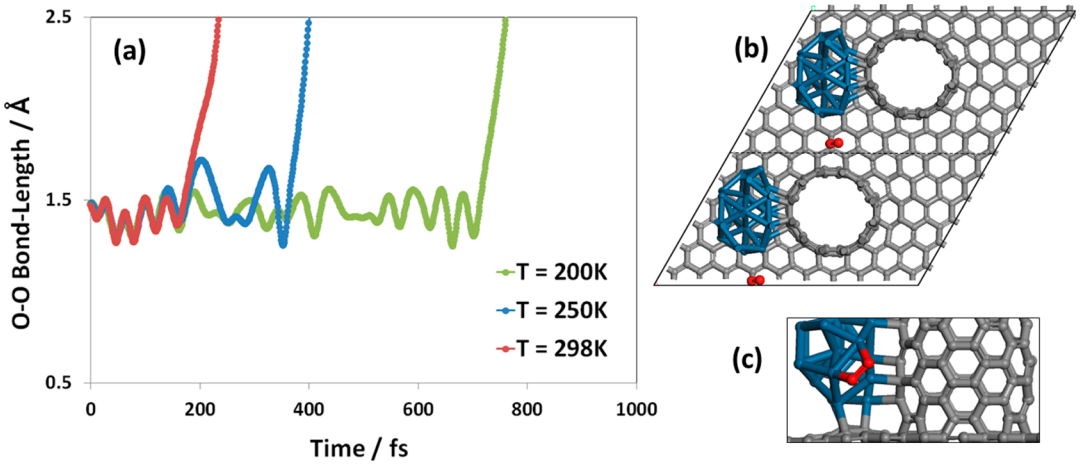

Figure 7. (a) O−O bond length as a function of time for the O_2 molecule interacting with Pt_{22}/NPG at (200 K, 10 atm.), (250 K, 13 atm.), and (298 K, 15 atm.). Time zero represents the time at which the molecule is first adsorbed onto the Pt_{22} nanoparticle. (b) Top view of two unit cells of the initial configuration of the O_2 molecule in the Pt_{22}/NPG system. (c) Bridge-site adsorption of O_2. Platinum atoms are blue, carbon atoms are gray, and oxygen atoms are red.

dx.doi.org/10.1021/cs5013798 | ACS Catal. 2015, 5, 215−224

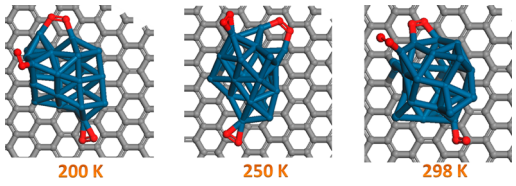

Figure 8. Final configuration of O_2 molecules on the Pt_{26}/graphite systems at (200 K, 10 atm), (250 K, 13 atm), and (298 K, 15 atm). Platinum atoms are blue, carbon atoms are gray, and oxygen atoms are red.

and 250 K, the bond length of the molecule oscillates in a wider range of values when adsorbed on the Pt_{22}/NPG system (red line). For example, the vibrational amplitude of the molecule adsorbed on the small-pore-size Pt_{22}/NPG system at 200 and 250 K prior to dissociation varies between 1.25 and 1.56 Å and 1.25−1.72 Å, respectively, compared with 1.34−1.50 and 1.26−1.61 Å in the larger-pore-size Pt_{26}/graphite system. These longer O−O oscillations may be responsible for the faster O_2 dissociation in Pt_{22}/NPG at 200 and 250 K compared with Pt_{26}/graphite. However, at 298 K, the O−O vibrational amplitude oscillates in the same range—between 1.26 and 1.80 Å in both systems—and dissociation is observed only on Pt_{22}/NPG. Given the presence of electron-rich regions in the small-pore-size Pt_{22}/NPG system, electronic charges of O_2 molecules adsorbed on this system may be different from those adsorbed on the larger-pore-size Pt_{26}/graphite (no electron-rich regions). As shown in the previous section, the presence of electron-rich regions may result in a larger amount of charge being transferred to adsorbed molecules, which debilitates their molecular bond and facilitates their dissociation.

At 298 K, no bond dissociation is observed after 8 ps of simulation for the larger-pore-size Pt_{26}/graphite system. To verify the hypothesis regarding charge transfer, charges were calculated as a function of the molecular bond length, for O_2 in Pt_{22}/NPG and Pt_{26}/graphite at the different (T, P) conditions (Figure 10). A direct relationship is found between the molecular bond length and the molecular charge: the longer the O−O bond, the more negative the molecular charge. At T = 200 K, data for the O_2 molecule in Pt_{22}/NPG fall under the same fitting line as that for the O_2 molecule in Pt_{26}/graphite (Figure 10, left). Thus, at that temperature, molecules with a given O−O bond length possess similar charges in both systems. This suggests that dissociation at 200 K is observed only in Pt_{22}/NPG as a result of the wider spectrum of charges being transferred to the adsorbed molecule in this system (−0.44|e$^-$| to −0.75|e$^-$|, compared with −0.53|e$^-$| to −0.69|e$^-$| in Pt_{26}/graphite), which leads to larger O−O bond length vibrational amplitudes that facilitate the breaking of the molecular bond. The spectrum of charges being transferred in the Pt_{22}/NPG system may be wider because of the presence of the neighboring electron-rich region interacting with the adsorbed molecule. Electrons in such a region are expected to have energies close to the Fermi energy of Pt_{22}/NPG,[3] and as shown in the previous section, the LUMO of O_2 lies below the Fermi energy of a Pt/graphite system, which allows for a spontaneous charge transfer from the electron-rich region to the molecule.

At T = 250 K, the range of charges being transferred to the adsorbed molecule in Pt_{22}/NPG is, again, slightly larger (−0.5|e| to −0.86|e|, compared with −0.48|e| to −0.78|e| in Pt_{26}/graphite), causing longer O−O bond length oscillations. But in addition, the fitting line for data corresponding to O_2 in Pt_{22}/NPG (red line in Figure 10, center) is slightly below the fitting line for the data corresponding to O_2 in Pt_{26}/graphite (blue line in Figure 10, center). This means that, on average, O_2 molecules with a given O−O bond length are slightly more negative when adsorbed on Pt_{22}/NPG (about 0.02|e$^-$| more negative). The more negative charge is also believed to be related to the presence of electron-rich regions in the small-pore-size Pt_{22}/NPG system. As the temperature is raised, migration of electrons to the confined region between the Pt cluster and the SWCNT may be facilitated, which results in a larger electronic density interacting with the adsorbed O_2 molecule. Consequently, at this intermediate temperature (T = 250 K), the effect of electron-rich regions on the reactivity of Pt_{22}/NPG is two-fold. First, there is a wider spectrum of charges being transferred to the O_2 molecule, which results in longer O−O bond length oscillations than those of the molecule adsorbed on the larger-pore-size Pt_{26}/graphite. Second, the presence of electron-rich regions in small-pore-size Pt_{22}/NPG helps to transfer a slightly larger amount of charges to adsorbed O_2 molecules for a given O−O bond length. The combination of these two factors results in an enhanced reactivity of Pt_{22}/NPG and dissociation of the O_2 molecule within a few hundred femtoseconds of adsorption. No dissociation is observed for molecules adsorbed on Pt_{26}/graphite after eight picoseconds of AIMD simulations under the same (T, P) conditions.

Finally, at 298 K, the O−O bond length oscillations (vibrational amplitudes) are very similar in both systems—Pt_{22}/NPG and Pt_{26}/graphite—as can be observed in Figure 9, right (~1.26−1.80 Å). However, the O_2 molecule adsorbed on Pt_{22}/NPG is more negative, on average (about 0.07|e$^-$|), than that adsorbed on Pt_{26}/graphite for the same O−O bond length (Figure 10, right). Therefore, at this higher temperature (T = 298 K), the presence of electron-rich regions in the system helps increasing the amount of charge transferred to adsorbed molecules compared with that transferred in the absence of

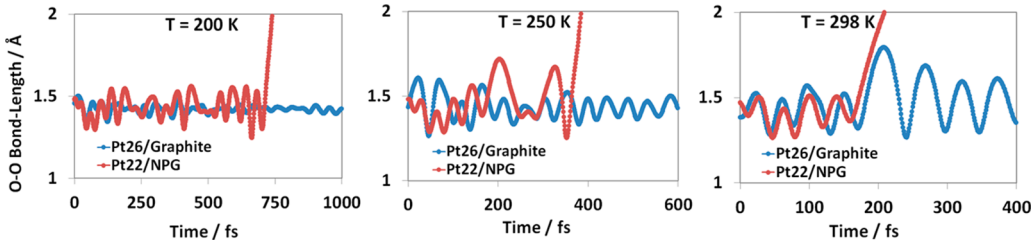

Figure 9. O−O bond lengths of the O_2 molecule adsorbed on Pt_{22}/NPG at different (T, P) conditions. Time zero represents the time at which the molecule is first adsorbed onto the Pt nanoparticle.

dx.doi.org/10.1021/cs5013798 | ACS Catal. 2015, 5, 215−224

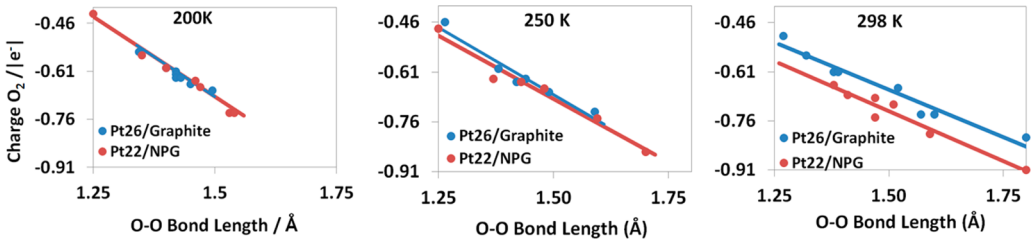

Figure 10. O_2 Charges as a function of the molecular bond length for O_2 in Pt_{22}/NPG and Pt_{26}/graphite at the different (T, P) conditions. The fitting line extends over the range in which bond lengths oscillate in each system.

these regions, which helps weaken the O−O bond and allows dissociation of the O_2 molecule after ∼180 fs after the initial adsorption. Again, no dissociation is observed for molecules adsorbed on larger-pore-size Pt_{26}/graphite after eight picoseconds of AIMD simulations under the same (T, P) conditions.

In summary, there is a clear effect of electron-rich regions on the reactivity of platinum-decorated carbon nanostructures toward the dissociation of O_2. When electron-rich regions are present at low and intermediate temperatures (200−250 K), a wider spectrum of charges is transferred to adsorbed molecules, which generates longer bond-length oscillations that facilitate the molecular dissociation. As the temperature increases (298 K), the effect of bond-length oscillations is less important as this becomes similar to that observed in systems with no electron-rich regions (Figure 9). However, elevated temperatures may facilitate a larger migration of electrons to the confined region between the Pt cluster and the SWCNT, which leads to larger electronic densities in the neighboring electron-rich region. As a result, adsorbed molecules interacting with it are, on average, more negative (Figure 10, center and right). As discussed above, the LUMO of the O_2 molecule is an antibonding orbital, and its filling facilitates the breaking of the O−O bond.

3.4. Adsorption and Dissociation of CH_4 in Pt/Decorated Microporous Structures. Results from AIMD simulations indicated that methane molecules interacting with a small-pore-size Pt_{22}/NPG system were found to adsorb onto the Pt_{22} cluster after 14170, 9533, 440, and 380 fs at (1000 K, 300 atm), (1100 K, 329 atm), (1200 K, 359 atm), and (1500 K, 449 atm), respectively. In all cases, the same initial configuration was used for the AIMD simulations, as shown in Figure 11, left. The first dehydrogenation takes place almost immediately upon adsorption of the molecule on the Pt cluster. In every case, the dehydrogenation takes place through the initial formation of Pt−C and Pt−H bonds. Each of these bonds originates in the same Pt atom, and eventually leads to the breaking of the corresponding C−H bond in the methane molecule (Figure 11, right). Similar mechanisms have been previously proposed for the catalytic dehydrogenation of alkanes using transition metals.[46,47] The dehydrogenation reaction takes place through a three-centered transition state in which the metal atom (M) interacts with both atoms of a C−H bond of the alkane, forming M−C and M−H bonds. The strength of the combined M−C and M−H bonds exceeds that of the C−H bond in the alkane, making the dehydrogenation process thermodynamically favorable.[46,47]

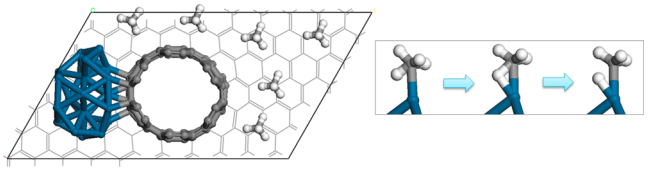

Figure 11. Left: Top view of unit cell representing the initial configuration for the AIMD simulations of CH_4 on Pt_{22}/NPG. Right: Dehydrogenation mechanism, in which the configuration in the middle is the three-centered transition state. Platinum atoms are blue, carbon atoms are gray, and hydrogen atoms are white.

Methane molecules interacting with the larger-pore-size Pt_{26}/graphite system (Figure 3b) at the same (T, P) conditions were also studied through AIMD simulations. The same initial configuration was used in every case, as shown in Figure S-2 (Supporting Information). No adsorption of CH_4 molecules on the Pt cluster was observed after 14 000 fs of simulation at (1200 K, 359 atm) and (1500 K, 449 atm). However, adsorption and dehydrogenation of one methane molecule was observed at (1100 K, 329 atm) after ∼12 500 fs. The dehydrogenation mechanism observed in this case was equivalent to that observed in the Pt_{22}/NPG system (Figure 11, right).

To investigate possible differences in the dehydrogenation process taking place on small-pore Pt_{22}/NPG vs the larger-pore Pt_{26}/graphite system, the C−H bond length of the adsorbed molecule was plotted as a function of time for each system at 1100 K (Figure 12, left). Time zero represents the time at which the methane adsorbs onto the Pt cluster (Pt$_{22}$ or Pt$_{26}$). In both cases, the C−H bond length at this time corresponds to 1.13 Å. The C−H bond length of the methane molecule adsorbed on Pt_{22}/NPG increases slightly more rapidly than that of the molecule adsorbed on Pt_{26}/graphite between C−H = 1.13 and 1.30 Å (approximate length at which the C−H bond breaks). Data in Figure 12, left, were fitted taking into account the time needed for the C−H bond to reach 1.30 Å after adsorption (5 fs in the case of Pt_{22}/NPG and 9 fs in the case of Pt_{26}/graphite), and a slightly larger slope corresponding to

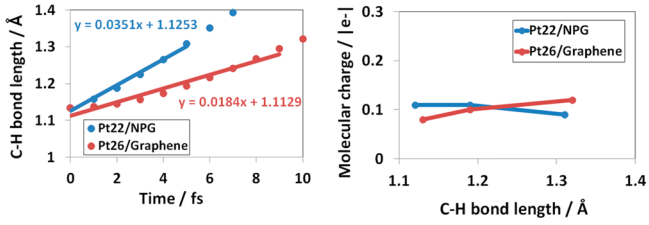

Figure 12. Left: C−H bond length of the adsorbed CH_4 molecule as a function of time for each system at 1100 K. The fitting line extends up to C−H = 1.3 Å, and time zero represents the time at which the methane adsorbs onto the Pt cluster. Right: Charge of the methane molecule as a function of the activated CH bond length.

dx.doi.org/10.1021/cs5013798 | ACS Catal. 2015, 5, 215−224

0.035 Å/fs is found in the case of Pt_{22}/NPG. However, differences calculated in Figure 12 are not significant, as the difference between dissociation times after adsorption is only 4 fs between the two systems. Charges of the methane molecules during dissociation were also calculated for three different C−H bond lengths and are plotted in Figure 12, right. In both cases (Pt_{22}/NPG and Pt_{26}/graphite), the charge of the adsorbed molecule is positive and around 0.1|e$^-$|. Thus, significant charge transfer from the Pt cluster to the CH_4 molecule is not evident during its first dehydrogenation. The barrier ($LUMO_{molecule} - E_{Fermi\text{-}Pt_{26}}$) calculated for transference of charge to CH_4 corresponds to ∼4.4 eV, which is a significantly high barrier that may explain the inability of the system to transfer electrons to the LUMO of methane molecules.

Even though electron-rich regions do not significantly affect the charge density of molecules with substantial ($LUMO_{molecule} - E_{Fermi}$) barriers, the confined nature of these regions may have a geometric effect on the reactivity of the system. For example, comparison of times required for molecular adsorption taking place on Pt_{22}/NPG and Pt_{26}/graphite suggests that shorter times are required on the small-pore-size Pt_{22}/NPG system. As discussed above, CH_4 is found to adsorb onto the Pt_{22}/NPG after 14 170, 9533, 440, and 380 fs at (1000 K, 300 atm), (1100 K, 329 atm), (1200 K, 359 atm), and (1500 K, 449 atm), respectively. Meanwhile, adsorption on Pt_{26}/graphite at (1200 K, 359 atm) and (1500 K, 449 atm) was not observed after 14 000 fs of AIMD simulations, and that at (1100 K, 329 atm) was observed after ∼12 500 fs. Dehydrogenation of molecules such as methyl cyclohexane has been carried out with higher catalytic activities than conventional Pt/SiO_2 when the Pt nanoparticles are confined in the pores of ordered SBA-15 templates.[32] This improved behavior was attributed to the better dispersion of Pt nanoparticles found inside the ordered SBA-15 template. In addition, different authors have found that the structure and pore size of zeolites influences the reaction rates inside the zeolite.[48]

To quantify geometric effects given by the spatial confinement of electron-rich regions, the mean free path of methane molecules was calculated from the AIMD simulations in Pt_{22}/NPG and Pt_{26}/graphite at the different (T, P) conditions. Mean free paths of individual molecules were calculated as the average distance traveled by the molecule between collisions with the support material. Subsequently, the mean free path of the system at a given (T, P) condition was calculated as the average of the individual mean free paths. Collisions were defined as $H_{methane}$−$C_{NPG\ (or\ graphite)}$ interactions occurring at distances below 1.28 Å, and $H_{methane}$−Pt interactions occurring at distances below 1.85 Å. These cutoff distances (1.28 and 1.85 Å) correspond to the sum of the covalent radii of the involved atoms (H−C and H−Pt) with a 12% increase to account for bond-length oscillations.

Table 1 shows calculated mean free path values for methane. On average, methane molecules travel 33.3 Å between collisions with the Pt_{22}/NPG system and 120.3 Å between collisions with Pt_{26}/graphite. Thus, the frequency of collisions is increased in the system with electron-rich regions (Pt_{22}/NPG) due to the more pronounced geometric confinement found in this case (pore size ∼0.56 nm vs ∼1 nm in Pt_{26}/graphite). Therefore, on the basis of the AIMD results, we conclude that even when the electron-rich regions do not interact with the molecules of interest, microporous NPG structures such as the one proposed on this work may enhance the reactivity of the metal clusters decorating the structure as a result of small pore sizes that increase the frequency of interaction between the catalyst and molecules.

Table 1. Calculated Mean Free Path Values for Methane Molecules in Pt_{22}/NPG and Pt_{26}/Graphite under Different (T, P) Conditions

	mean free path (Å)	
temp (K)	Pt_{22}/NPG	Pt_{26}/graphite
1000	24.9	
1100	34.3	131.1
1200	44.5	109.7
1500	29.3	120.1
average	33.3	120.3

4. CONCLUSIONS

A Pt_{22}/NPG structure exhibiting electron-rich regions was proposed as a model nanostructured catalyst for the dissociation of molecules in the gas phase. Electron-rich regions are formed in this system through close interactions between the Pt cluster and SWCNTs (separation ∼5.5 Å). In the first part of this work, O_2, CO, and N_2 molecules were adsorbed on a Pt_{26} cluster with and without the presence of electron-rich regions. Charges transferred to molecules in electron-rich regions during adsorption are up to 35% larger compared with those of molecules adsorbed on the cluster with no presence of electron-rich regions. In addition, bond lengths of adsorbed molecules are up to 0.84% longer. Therefore, molecules in electron-rich regions exhibit weaker molecular bonds, and it is expected that smaller barriers will be required for their dissociation. It was also found that the energy difference ($LUMO_{molecule} - E_{Fermi\text{-}catalyst}$) provides the barrier required for charge transfer to the molecule. Consequently, it is possible to selectively enhance catalytic reactions by efficiently coupling the Fermi energy of the catalyst (by changing the metal particle decorating the NPG) with the LUMO orbital of the molecule of interest. In that way, a larger amount of charges can be transferred to LUMO antibonding orbitals of molecules, weakening their molecular bonds.

In the second part of this work, AIMD simulations of O_2 molecules interacting with the proposed Pt/NPG catalysts were performed. These simulations were compared with those of O_2 molecules interacting with a Pt_{26}/graphite system at the same (T, P) conditions. Pt_{26}/graphite represents an ordered carbon-based material with larger pore sizes than those in NPG (∼1 nm vs ∼0.56 nm in NPG), and consequently, it does not possess electron-rich regions. A clear effect of electron-rich regions on the reactivity of platinum-decorated microporous carbon was observed. First, it may help by allowing a wider range of electrons being transferred to adsorbed molecules, which generates longer bond-length oscillations that facilitate the molecular dissociation. In addition, at higher temperatures, a larger migration of electrons to the confined region between the Pt cluster and the SWCNT may be possible, which results in adsorbed molecules with more negative charges. The additional charge goes to the antibonding LUMO of the O_2 molecule, facilitating the breaking of its O−O bond.

Finally, the dehydrogenation of methane was also studied on the proposed Pt/NPG system using AIMD simulations. In this case, the calculated ($LUMO_{molecule} - E_{Fermi\text{-}catalyst}$) barrier is significantly high, corresponding to 4.4 eV. As a result, electron-rich regions do not significantly affect the charge density of

dx.doi.org/10.1021/cs5013798 | ACS Catal. 2015, 5, 215−224

methane molecules; however, smaller times required for molecular adsorption on Pt_{22}/NPG than on Pt_{26}/graphite and shorter mean free paths existent in the former system are shown to be related to the confined geometries. Ordered Pt/NPG structures such as the one proposed on this work may display enhanced reactivity, even when electron-rich regions do not interact with the molecules of interest, as a result of the good dispersion of Pt clusters on the material and small pore sizes that increase the frequency of interaction between catalysts and molecules.

In summary, the Pt/NPG catalyst proposed in this work is a good candidate for the efficient dissociation of molecules in gas phase. The presence of electron-rich regions in the material enhances its reactivity toward the dissociation of diatomic molecules. In addition, its reactivity may be tailored by effectively coupling the energy of electrons in electron-rich regions with that of antibonding orbitals of molecules of interest. Such coupling allows additional transference of electrons to adsorbed molecules, weakening molecular bonds and facilitating molecular dissociations. Moreover, the ordered nature of the catalyst and the small pore size of the host material may also have a geometric effect on reactivity, even in cases when electron-rich regions do not effectively interact with the LUMO of molecules of interest.

■ ASSOCIATED CONTENT

Supporting Information

The following file is available free of charge on the ACS Publications website at DOI: 10.1021/cs5013798.

Figures illustrating the structure of the Pt-decorated NPG model proposed in Figure 2a after DFT optimization and showing the initial configuration for the AIMD simulations of CH_4 on Pt_{26}/graphite (PDF)

■ AUTHOR INFORMATION

Corresponding Author

*E-mail: balbuena@tamu.edu.

Notes

The authors declare no competing financial interest.

■ ACKNOWLEDGMENTS

Computational resources from Texas A&M Supercomputing Center, Brazos Supercomputing Cluster at Texas A&M University and from Texas Advanced Computing Center at UT Austin are gratefully acknowledged.

■ REFERENCES

(1) Martinez de la Hoz, J. M.; Balbuena, P. B. *Phys. Chem. Chem. Phys.* **2013**, *15*, 1647−1654.
(2) Martínez de la Hoz, J. M.; Balbuena, P. B. *J. Phys. Chem. C* **2011**, *115*, 21324−21333.
(3) Martinez de la Hoz, J. M.; Ramirez-Caballero, G. E.; Balbuena, P. B. *J. Phys. Chem. C* **2013**, *117*, 18406−18413.
(4) Pérez-González, O.; Zabala, N.; Aizpurua, J. *New J. Phys.* **2011**, *13*, 083013−16.
(5) Ramírez-Caballero, G.; Martínez de la Hoz, J. M.; Balbuena, P. B. *J. Phys. Chem. Lett.* **2012**, *3*, 818−825.
(6) Ramírez-Caballero, G. E.; Balbuena, P. B. *Chem. Phys. Lett.* **2011**, *507*, 117−121.
(7) Ramirez-Caballero, G. E.; Mathkari, A.; Balbuena, P. B. *J. Phys. Chem. C* **2011**, *115*, 2134−2139.
(8) Wu, L.; Duan, H.; Bai, P.; Bosman, M.; Yang, J. K. W.; Li, E. *ACS Nano* **2012**, *7*, 707−716.
(9) Zhao, K.; Troparevsky, M. C.; Xiao, D.; Eguiluz, A. G.; Zhang, Z. *Phys. Rev. Lett.* **2009**, *102*, 186804−4.
(10) Zuloaga, J.; Prodan, E.; Nordlander, P. *Nano Lett.* **2009**, *9*, 887−891.
(11) Dimitrakakis, G. K.; Tylianakis, E.; Froudakis, G. E. *Nano Lett.* **2008**, *8*, 3166−3170.
(12) Zhu, Y.; Li, L.; Zhang, C.; Casillas, G.; Sun, Z.; Yan, Z.; Ruan, G.; Peng, Z.; Raji, A.-R. O.; Kittrell, C.; Hauge, R. H.; Tour, J. M. *Nat. Commun.* **2012**, *3*, 1225−1232.
(13) Paul, R. K.; Ghazinejad, M.; Penchev, M.; Lin, J.; Ozkan, M.; Ozkan, C. S. *Small* **2010**, *6*, 2309−2313.
(14) Peigney, A.; Laurent, Ch.; Flahaut, E.; Bacsa, R. R.; Rousset, A. *Carbon* **2001**, *39*, 507−514.
(15) Du, F.; Yu, D.; Dai, L.; Ganguli, S.; Varshney, V.; Roy, A. K. *Chem. Mater.* **2011**, *23*, 4810−4816.
(16) Fan, Z.; Yan, J.; Zhi, L.; Zhang, Q.; Wei, T.; Feng, J.; Zhang, M.; Qian, W.; Wei, F. *Adv. Mater.* **2010**, *22*, 3723−3728.
(17) Lin, J.; Zhong, J.; Bao, D.; Reiber-Kyle, J.; Wang, W. *J. Nanosci.Nanotechnol.* **2012**, *12*, 1770−1775.
(18) Lee, J. M.; Choung, J. W.; Yi, J.; Lee, D. H.; Samal, M.; Yi, D. K.; Lee, C.-H.; Yi, G.-C.; Paik, U.; Rogers, J. A.; Park, W. I. *Nano Lett.* **2010**, *10*, 2783−2788.
(19) Ma, Y.; Sun, L.; Huang, W.; Zhang, L.; Zhao, J.; Fan, Q.; Huang, W. *J. Phys. Chem. C* **2011**, *115*, 24592−24597.
(20) Li, Y.; Zhou, W.; Wang, H.; Xie, L.; Liang, Y.; Wei, F.; Idrobo, J.-C.; Pennycook, S. J.; Dai, H. *Nat. Nanotechnol.* **2012**, *7*, 394−400.
(21) Zhu, X.; Ning, G.; Fan, Z.; Gao, J.; Xu, C.; Qian, W.; Wei, F. *Carbon* **2012**, *50*, 2764−2771.
(22) Lee, D. H.; Lee, J. A.; Lee, W. J.; Choi, D. S.; Lee, W. J.; Kim, S. O. *J. Phys. Chem. C* **2010**, *114*, 21184−21189.
(23) Gálvez, M.; Calvillo, L.; Alegre, C.; Sebastián, D.; Suelves, I.; Pérez-Rodríguez, S.; Celorrio, V.; Pastor, E.; Pardo, J.; Moliner, R.; Lázaro, M. *Catalysts* **2013**, *3*, 671−682.
(24) Ding, J.; Chan, K.-Y.; Ren, J.; Xiao, F. S. *Electrochim. Acta* **2005**, *50*, 3131−3141.
(25) Kong, L.-B.; Li, H.; Zhang, J.; Luo, Y.-C.; Kang, L. *Appl. Surf. Sci.* **2010**, *256*, 6688−6693.
(26) Ishii, A.; Yamamoto, M.; Asano, H.; Fujiwara, K. *J. Phys.: Conf. Series* **2008**, *100*, 052087−5.
(27) Eichler, A.; Hafner, J. *Phys. Rev. Lett.* **1997**, *79*, 4481−4484.
(28) Marek, G.; Eichler, A.; Hafner, J. *J. Phys.: Condens. Matter* **2004**, *16*, 1141−1164.
(29) Stewart, R. B.; Jacobsen, R. T.; Wagner, W. *J. Phys. Chem. Ref. Data* **1991**, *20*, 917−1021.
(30) Xu, J.; Zheng, A.; Wang, X.; Qi, G.; Su, J.; Du, J.; Gan, Z.; Wu, J.; Wang, W.; Deng, F. *Chem. Sci.* **2012**, *3*, 2932−2940.
(31) An, W.; Zeng, X. C.; Turner, C. H. *J. Chem. Phys.* **2009**, *131*, 174702−11.
(32) Chen, A.; Zhang, W.; Li, X.; Tan, D.; Han, X.; Bao, X. *Catal. Lett.* **2007**, *119*, 159−164.
(33) Kresse, G.; Furthmüller, J. *Phys. Rev. B* **1996**, *54*, 11169−11186.
(34) Kresse, G.; Furthmuller, J. *Comput. Mater. Sci.* **1996**, *6*, 15−50.
(35) Kresse, G.; Hafner, J. *Phys. Rev. B* **1993**, *48*, 13115−13118.
(36) Kresse, G.; Hafner, J. *Phys. Rev. B* **1993**, *47*, 558−561.
(37) Kresse, G.; Hafner, J. *Phys. Rev. B* **1994**, *49*, 14251−14269.
(38) Hammer, B.; Hansen, L. B.; Nørskov, J. K. *Phys. Rev. B* **1999**, *59*, 7413−7421.
(39) Blöchl, P. E. *Phys. Rev. B* **1994**, *50*, 17953−17979.
(40) Kresse, G.; Joubert, D. *Phys. Rev. B* **1999**, *59*, 1758−1775.
(41) Monkhorst, H. J.; Pack, J. D. *Phys. Rev. B* **1976**, *13*, 5188−5192.
(42) Henkelman, G.; Arnaldsson, A.; Jónsson, H. *Comput. Mater. Sci.* **2006**, *36*, 354−360.
(43) Sanville, E.; Kenny, S. D.; Smith, R.; Henkelman, G. *J. Comput. Chem.* **2007**, *28*, 899−908.
(44) Fukui, K.; Yonezawa, T.; Shingu, H. *J. Chem. Phys.* **1952**, *20*, 722−725.
(45) Hammer, B.; Norskov, J. K. *Surf. Sci.* **1995**, *343*, 211−220.
(46) Nizovtsev, A. S. *J. Comput. Chem.* **2013**, *34*, 1917−1924.
(47) Zaera, F. *Appl. Catal. A-Gen.* **2002**, *229*, 75−91.

(48) Bhan, A.; Gounder, R.; Macht, J.; Iglesia, E. *J. Catal.* **2008**, *253*, 221−224.